Magnetic Tuning of the Photovoltaic Effect in Silicon-Based Schottky Junctions

*Shuanhu Wang, Wenxin Wang, Lvkuan Zou, Xu Zhang, Jianwang Cai, Zhigang Sun, Baogen Shen, and Jirong Sun**

In general, work on the magnetic effect of the conventional semiconductors,[1–5] which has been the focus of intensive study in recent years, can be divided into three categories. In the first category, the generation/manipulation of spin-polarized current has been achieved via circularly polarized light excitation,[2] electron tunneling,[3] spin pumping,[4] and Seebeck spin tunneling,[5] and various effects such as the spin Hall effect[6] and the spin torque transfer effect[7] have been reported. The second category of work is aimed at the modification of the charge-transport process in semiconductors. It has been reported that unevenly distributed charge carriers in Si are susceptible to a magnetic field.[8,9] There are also indications for positive magnetoresistance arising from the shrinkage of the electron wavefunction of the impurity states in a magnetic field.[9,10] The last category of work is the p–n junction or Schottky junction. As reported, a magnetic field drives the turn-on voltage of diodes considerably upward, yielding magnetically tunable rectifying behaviors.[11]

In most of the previous work, the magnetic effect was produced by direct tuning, i.e., applying a magnetic field directly to a semiconductors to modify the kinetic/dynamic behaviors of the charge carriers.[8,11] In this case, usually a field on the magnitude of Tesla is required to get significant effects. Obviously, a low-field magnetic effect is no doubt more important for either fundamental research or practical application. Unfortunately, it is hardly achieved because of the insensitivity of the conventional semiconductors to magnetic field. Compared with semiconductors, soft ferromagnetic (FM) materials are much more susceptible to magnetic fields. Through the coupling of the FM material with semiconductor, an indirect approach for magnetic tuning could be developed, i.e., tuning the latter by changing the former. This is particularly important noting the fact that the search for suitable FM metals is relatively easier.

It is well established that Permalloy ($Ni_{80}Fe_{20}$) (Py) is an FM material with a very low coercive force field, usually a few oersteds, and a large anisotropic magnetoresistance, AMR ≈ 2% at room temperature.[12] $Ni_{65}Co_{35}$ (NC) is another representative AMR material, with an AMR up to 5% at room temperature.[13] The work functions of the Py and the NC are ca. 4.7 eV and ca.4.9 eV, respectively. Si is the mostly studied semiconductor. As tabulated, the electron affinity of Si is ca. 4.3 eV when electron-doped to ca. 10^{15} cm^{-3} and ca. 5.0 eV when hole-doped to 10^{15} cm^{-3}. Due to the difference in work function (electron affinity), a strong coupling can be created between Si and an FM material when they form a Schottky junction (FM/Si). An important feature of the Schottky junction is the photovoltaic effect: illuminating the junction by photons with an energy higher than the interface barrier or bandgap, a photocurrent or photovoltage can be generated across the two poles of the diode.[14] Here, we report a study on the lateral photovoltaic effect for FM/Si junctions, focusing on its magnetic tunability. Remarkably, the anisotropic photovoltage, driven by a field of several oersteds, appears not only in the FM layer but also in the Si, and its relative change is much larger in the latter than in the former. In addition to the lateral photovoltaic effect, a planar Hall photovoltage, a transverse photovoltaic effect, is also detected in the FM layer. Key factors affecting the magnetic effect are determined. The present work demonstrates an effective tuning of the electronic processes in Si by very low magnetic fields.

Six FM/Si junctions were prepared by depositing the FM strip, with an easy axis along its short direction, above n- or p-type Si substrates (see the Experimental Section for details). An easy axis is an energetically favorable direction of spontaneous magnetization. All the junctions exhibit typical diode behaviors that can be described by the Shockley equation (Figure S1 in the Supporting Information). As expected, the turn-on direction reverses for FM/n-Si and FM/p-Si junctions, indicating the opposite directions of the built-in electric fields in these two kinds of junction. The interfacial barrier, Φ_B, which is deduced from the current–voltage characteristics and the depletion layer width, X_D, which is derived from the capacitance–voltage relations, are tabulated in **Table 1**. As expected, both are much larger for the FM/n-Si junctions than for the FM/p-Si junction. The introduction of a non-magnetic Ta buffer layer in Ta/NC/Ta/n-Si causes a reduction in Φ_B, due to the similarity of the work functions of Ta and n-Si.

Figure 1a shows a sketch of the experimental setup. When the junction is illuminated by a laser beam at one end, a lateral photovoltage, V_{LP}, is generated and collected by a pair of electrodes on the FM layer or the Si substrate. Here, the illuminated position was set to $x = 0$. Fixing one electrode at $x_0 = 4.5$ mm, near the laser spot, while shifting another

S. Wang, L. Zou, X. Zhang, Prof. J. Cai, Prof. B. Shen, Prof. J. Sun
Beijing National Laboratory for Condensed Matter Physics and Institute of Physics
Chinese Academy of Sciences
Beijing 100190, PR China
E-mail: jrsun@iphy.ac.cn
W. Wang, Prof. Z. Sun
State Key Laboratory of Advanced Technology for Materials Synthesis and Processing
Wuhan University of Technology
Wuhan 430070, PR China

DOI: 10.1002/adma.201403868

Table 1. Junction parameters.

	Φ_B [eV]	X_D [μm]	$\alpha^{\perp}$ [mm^{-1}]	ϕ [$\times 10^{14}$ mm^{-2} s^{-1}]	AMV of Si ($\delta = 9$ mm) [%]	AMV of film ($\delta = 9$ mm) [%]	AMR [%]
Py/n-Si(1)	0.60 ± 0.01	0.61 ± 0.02	0.084 ± 0.001	4.2 ± 0.1	−0.50	1.30	1.46
Py/p-Si	0.07 ± 0.01	0.22 ± 0.01	0.256 ± 0.003	4.8 ± 0.2	−1.00	0.49	0.75
NC/n-Si(1)	0.59 ± 0.01	0.63 ± 0.02	0.038 ± 0.001	24 ± 1	−0.47	1.53	1.82
NC/p-Si	0.06 ± 0.01	0.20 ± 0.01	0.190 ± 0.002	16 ± 1	−3.24	1.11	1.51
Ta/NC/Ta/n-Si(1)	0.05 ± 0.01	0.14 ± 0.01	0.370 ± 0.004	3.6 ± 0.2	−1.81	1.40	1.79
Py/n-Si(2)	0.57 ± 0.01	>10	0.217 ± 0.002	0.56 ± 0.03	0	1.55	1.58

electrode in the x direction to different separations, $\delta = x - x_0$, we obtained the $V_{LP} - x$ relations for the FM layer and the Si substrate in Figures 1b,c. Two features can be identified from these results. The first is the monotonic growth of V_{LP} with δ and the second is the sign reversal of V_{LP} from the n-type to the p-type junctions and from the FM layer to the Si substrate. These are the typical features of the lateral photovoltaic effect.

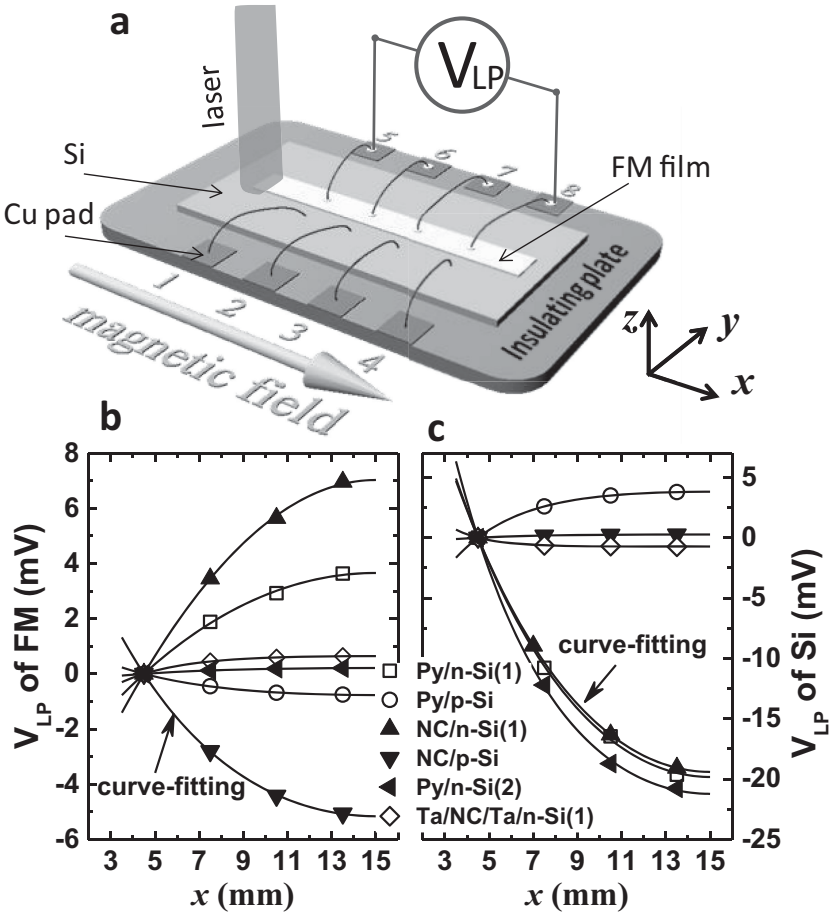

Figure 1. a) A sketch of experiment setup. Cu pads were connected to the FM film by silver paint and to Si substrate by Al wire bonding. The welding spot is 1 mm away from the film edge in the y direction. b) The lateral photovoltage V_{LP} of the FM film and Si substrate as a function of electrode position. The symbols are the experimental data and the lines are the results of curve fitting based on Equation 2. The laser power adopted in the experiments was 30 mW (beam size = 2 mm × 2 mm).

As is well established, photoexcited electrons and holes will be separated by the built-in field, accumulating at the two poles of the junction. Driven by the lateral electric field and concentration gradient, the accumulated photocarriers will then drift out of the illuminated region, forming two oppositely directed currents in the FM layer and the Si substrate. A simple analysis of the energy-band structure of the FM/Si junction indicates that the photocarriers will be holes (electrons) in the FM (n-Si) side and electrons (holes) in the FM (p-Si) side. Therefore, the V_{LP} of the FM layer and the Si substrate always exhibit opposite signs.

Remarkably, the V_{LP} of the junction shows a strong dependence on magnetic field. **Figure 2**a,b present the V_{LP} of the Py/n-Si(1) and Py/p-Si junctions, measured in a field applied along the hard axis of the FM layer (x-axis). Along the hard axis, it is hard to magnetize the film. Here, only the results obtained by descending field are presented. The field-ascending process yields similar data. For the Py/n-Si(1) junction; for example, the V_{LP} of the Py layer grows rapidly while H deviates from zero, and saturates above a threshold field of 5 Oe. This behavior could be ascribed to the reorientation of the magnetic moment. As shown in Figure 2c, the magnetic moment of the Py layer rotates with applied field when the field is low and saturates above 5 Oe. Fascinatingly, the absolute value of V_{LP} of the non-magnetic Si also shows a variation with applied field, decreasing in magnitude as H increases. This result indicates that while the magnetic field enhances the V_{LP} of the FM layer, it depresses the V_{LP} of the Si. Similar phenomena are observed in all FM/n-Si junctions except for the one formed by lightly electron-doped Si, although the detailed V_{LP}–H dependence varies from sample to sample. The magnetic effect is also observed in FM/p-Si, and the absolute value of V_{LP} varies in the same way as that in FM/n-Si.

A distinct feature of the magnetic effect is its dependence on electrode separation. As shown in Figure 2d, the normalized

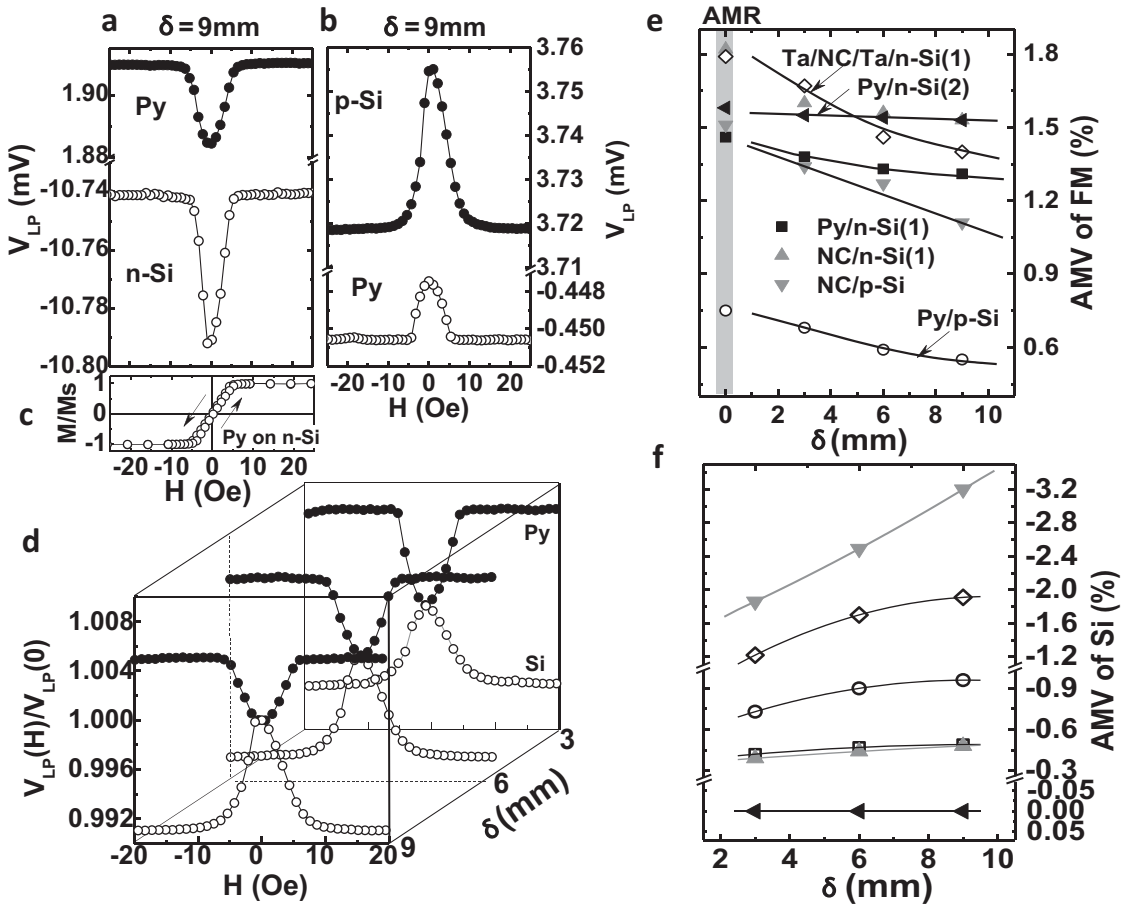

Figure 2. a,b) Lateral photovoltage as a function of magnetic field, measured at the n-Si/Py (a) and the p-Si/Py (b) junctions. c) Normalized magnetization of the Py layer, measured at room temperature. An external magnetic field is applied perpendicular to the easy magnetization axis. d) Normalized V_{LP}–H relations of the Py/p-Si junction, measured for different electrode separations, δ. e,f) AMV–δ relation of the FM layer and the Si substrate, measured for different FM/Si junctions. The AMR values of the FM layers are presented in the shaded area of (e) for comparison. The laser power was 30 mW.

photovoltage $V_{LP}(H)/V_{LP}(0)$ decreases with δ for the FM layer and increases with δ for the Si substrate. Denoting V_{LP} as $V_{LP}^{\perp}$ when it is recorded without a magnetic field (the easy axis of the FM layer is the y-axis) and $V_{LP}^{\parallel}$ when it is measured above the saturation field along the x-axis, we define an anisotropic magnetic photovoltage AMV = $(V_{LP}^{\parallel} - V_{LP}^{\perp})/V_{LP}^{\parallel}$. Figure 2e,f show the AMV as a function of δ. The first remarkable observation is the different dependence of the AMVs of the FM layer and Si substrate on δ, decreasing for the former (Figure 2e) but increasing for the latter (Figure 2f). The second remarkable observation is that the AMV of Si can achieve values much larger than that of the FM layer. According to Figure 2f, the largest value is ca. 3.2% for Si, appearing when δ = 9 mm, whereas the maximal AMV of the NC film is below ca. 1.4%. Extrapolating the AMV–δ relation to $\delta \to 0$, we found that the AMV of the FM layer approaches a value close to the corresponding AMR (Figure 2e). This result suggests that the AMV may share the same origin as the AMR, i.e., anisotropic magnetic scattering of charge carriers. A preliminary explanation could be that the reorientation of the magnetic moment affects the resistivity of the FM layer and, thus, the lateral diffusion/drift of the photocarriers, while the non-magnetic Si becomes magnetically susceptible through coupling to the FM layer.

In the above experiments, the AMV of Si is detected by two electrodes that are 1 mm away from the FM film. However, the photovoltage collected from different locations of the Si substrate could be different. **Figure 3**a shows the spatial distribution of the electrical potential on Si, obtained by finite element analysis. To check how far this magnetic response can be maintained, we measured the V_{LP} of Si while varying the distance of the two electrodes from the FM layer (d) but fixing their separation to δ = 9 mm, as sketched in Figure 3a. As shown by the AMV–d relation in Figure 3b, although the AMV decays with distance from the FM layer, it is still quite prominent even when d = 10 mm, i.e., the AMV of Si has a long-range nature.

The AMV is a longitudinal photoelectric effect, appearing when carrier transport is modified by an applied field. We also observed a tunable transverse photovoltaic effect. **Figure 4** presents the planar Hall photovoltage, V_{PHP}, collected from two transversely aligned electrodes while applying magnetic field at an angle of θ with the Py strip (Figure 4a). Again, a strong dependence of the photovoltage on H is observed for the Py

layers in both the Py/n-Si (left panel of Figure 4b) and Py/p-Si (right panel of Figure 4b) junctions, as demonstrated by the oscillating $V_{PHP} - H$ curve, for $\theta = 0°$, or the butterfly-shaped $V_{PHP} - H$ curve, for $\theta = 45°/135°$. A further analysis shows that the $V_{PHP} - \theta$ relation, extracted from the $V_{PHP} - H$ curves well above the saturation field (>5 Oe), can be described by:

$$V_{PHP} = k \sin 2\theta \tag{1}$$

adopting the k of 11.5 μV for Py/n-Si and −3.0 μV for Py/p-Si (Figure 4c). This result indicates that the transverse photovoltage shares the same mechanism as the planar Hall effect. On the analogy of the planar Hall effect, $k = (\rho_{Py}^{\parallel} - \rho_{Py}^{\perp}) J_{ph}/2$ where J_{ph} is the photocurrent through the Py layer, $\rho_{Py}^{\parallel}$ and $\rho_{Py}^{\perp}$ are the resistivities of the Py layer when the magnetic moment aligns along or normal to the measuring current, respectively. Since the direction of J_{ph} is opposite in Py/n-Si(1) and Py/p-Si, k changes sign from the former to the latter. The complex $V_{PHP} - H$ relation below the saturation field could be an effect of the reorientation of the magnetic moment. A weak $V_{PHP} - H$ dependence, about one tenth of that of the FM layer in magnitude, is also observed in Si (not shown), probably stemming from the short-circuit effect due to the close connection of Si with Py.

Without an applied field, the magnetic moment of the FM layer aligns along the y-axis of the sample (Figure 1a). According to Niu et al.,[15] the photovoltage in this case can be described by:

$$V_{LP}^{\perp}(x_0,\delta) = \frac{wq\phi\rho_M^{\perp}}{d_M\alpha_{FM}^{\perp}} \frac{[\cosh\alpha_{FM}^{\perp}(L-x_0) - \cosh\alpha_{FM}^{\perp}(L-x_0-\delta)]}{\sinh\alpha_{FM}^{\perp}L + w\alpha_{FM}^{\perp}\cosh\alpha_{FM}^{\perp}L} \tag{2}$$

where x_0 and $(x_0 + \delta)$ are the coordinates of the two electrodes for the electric measurements, $\rho_M^{\perp}$ and d_M are, respectively, the resistivity and thickness of the M component of the junction, ϕ is the concentration of excited electron–hole pairs per second, $w = 2$ mm is the beam size of the laser, and $L = 17$ mm is the long dimension of the film. $\alpha_{FM}^{\perp}$ has the form of:

$$\alpha_{FM}^{\perp} = \sqrt{\frac{eJ_s}{nk_BT}\left(\frac{\rho_{FM}^{\perp}}{d_{FM}} + \frac{\rho_{Si}}{d_{Si}}\right)} \tag{3}$$

where n and J_S are the ideality factor and saturation current of the junction, respectively. An excellent fitting of the experiment results to Equation 2 is obtained when adopting the fitting parameters n and $\alpha_{FM}^{\perp}$ in Table 1. The largest and smallest $\alpha_{FM}^{\perp}$ s are 0.37 mm^{-1} and 0.038 mm^{-1}, respectively, appearing in the Ta/NC/Ta/n-Si(1) and NC/n-Si(1) junctions. Here, $\alpha_{FM}^{\perp}$ determines the decay of V_{LP} with $\delta = x - x_0$, and a large $\alpha_{FM}^{\perp}$ implies a rapid damping. According to Equation 3, $\alpha_{FM}^{\perp}$ is proportional to $\sqrt{J_s}$. A large $\alpha_{FM}^{\perp}$ implies a large J_S, which means a severe recombination of the non-equilibrium charge carriers. ϕ quantifies the quantum efficiency of the photoexcitation. It is in the order of 10^{14} mm^{-2} s^{-1} under a laser power of 30 mW.

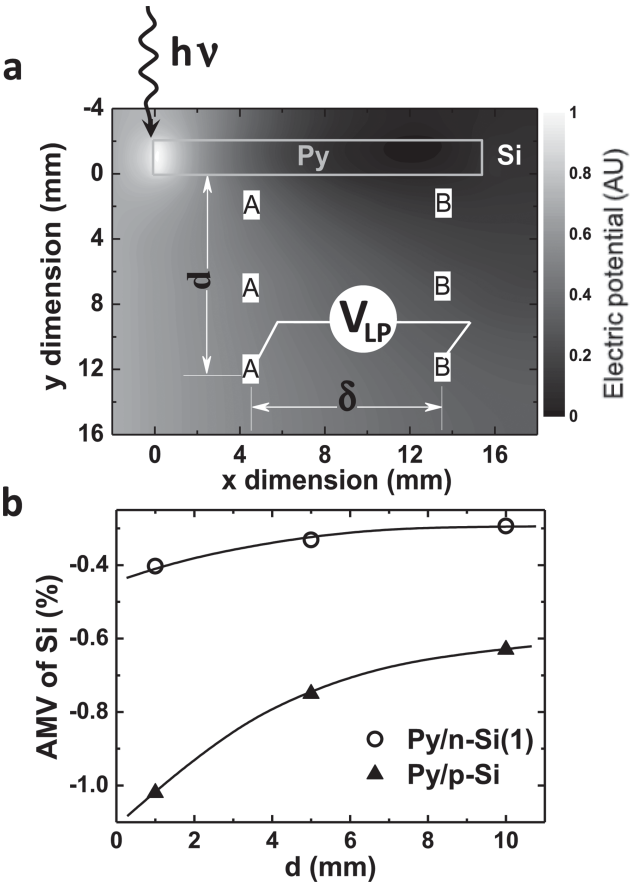

Figure 3. a) Distribution of the electrical potential on the x–y plane of Si, obtained by finite element analysis. b) AMV of the Si substrate in the Py/n-Si and Py/p-Si junctions, collected from the electrode separation of $\delta = 9$ mm and different distances away from film. The laser power was 30 mW.

In fact, the magnetic effect can be described by Equation 2. A direct calculation leads to:

$$\begin{aligned} AMV &= \frac{V_{LP}^{\parallel}(x_0,\delta) - V_{LP}^{\perp}(x_0,\delta)}{V_{LP}^{\parallel}(x_0,\delta)} \\ &= 1 - \frac{\rho_M^{\perp}}{\rho_M^{\parallel}} \frac{f(\alpha_{FM}^{\perp},x_0,\delta)}{f(\alpha_{FM}^{\parallel},x_0,\delta)} \end{aligned} \tag{4}$$

where $f(\alpha_{FM}^{\parallel},x_0,\delta) = \dfrac{\cosh\alpha_{FM}^{\parallel}(L-x_0) - \cosh\alpha_{FM}^{\parallel}(L-x_0-\delta)}{\alpha_{FM}^{\parallel}(\sinh\alpha_{FM}^{\parallel}L + w\alpha_{FM}^{\parallel}\cosh\alpha_{FM}^{\parallel}L)}$.

AMV is generally non-vanishing since $\rho_{FM}^{\parallel} > \rho_{FM}^{\perp}$ and $\alpha_{FM}^{\parallel} > \alpha_{FM}^{\perp}$ for the FM layers studied here. A direct calculation indicates that $f(\alpha_{FM}^{\perp},x_0,\delta)/f(\alpha_{FM}^{\parallel},x_0,\delta) > 1$, and grows monotonically with δ for any $x_0 < x < L$ when $\alpha_{FM}^{\parallel} > \alpha_{FM}^{\perp}$. This implies that the AMV of the FM layer is always smaller than the AMR ($AMV = 1 - \dfrac{\rho_{FM}^{\perp}}{\rho_{FM}^{\parallel}} \dfrac{f(\alpha_{FM}^{\perp},x_0,\delta)}{f(\alpha_{FM}^{\parallel},x_0,\delta)} < 1 - \dfrac{\rho_{FM}^{\perp}}{\rho_{FM}^{\parallel}} = AMR$), and monotonically decreases with δ. Setting x to x_0 and L to ∞, we have the formula $AMV = 1 - \dfrac{\rho_{FM}^{\perp}}{\rho_{FM}^{\parallel}} \exp[(\alpha_{FM}^{\parallel} - \alpha_{FM}^{\perp})x_0]$. In the limiting case

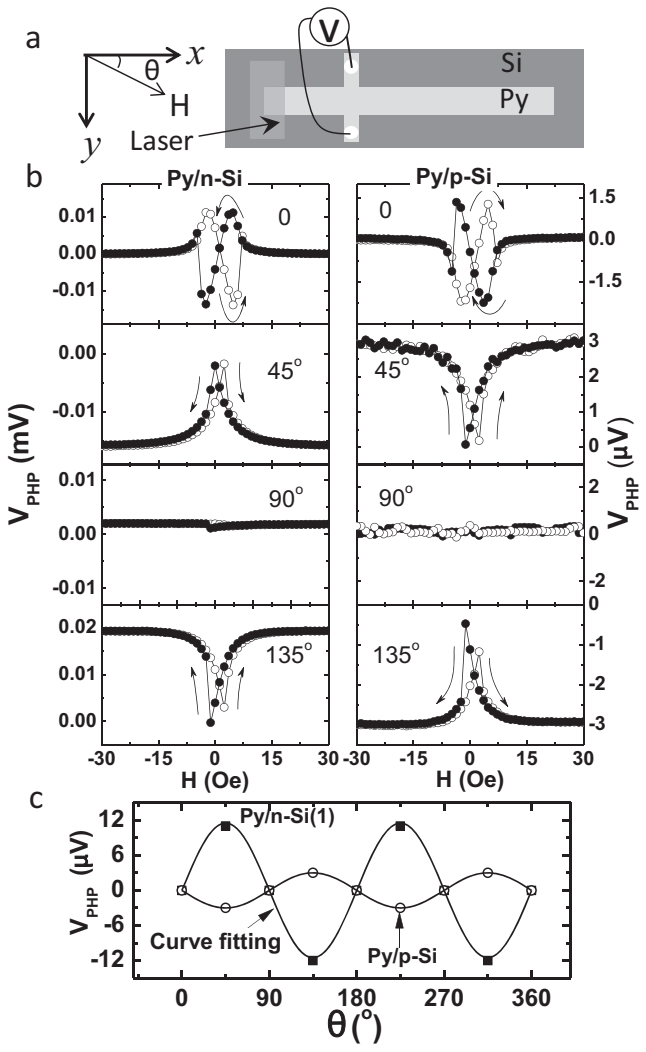

Figure 4. a) Experimental setup for the planar Hall photovoltage measurement. The Py strip was 0.2 mm in width. b) Dependence of the planar Hall photovoltage on magnetic field for the Py layers of Py/n-Si (left panel) and Py/p-Si (right panel). The labels mark the angles between the applied field and the Py strip. The curves denoted by the filled and open symbols were recorded in the field descending and ascending processes, respectively. c) The planar Hall photovoltage as a function of the angle between the magnetic moment and the Py strip.

of $x_0 = 0$, AMV = AMR. These inferences are confirmed by the experimental results shown in Figure 2e.

For the Si substrate, Equation 4 reduces to AMV = $1-f(\alpha_{FM}^{\perp},x_0,\delta)/f(\alpha_{FM}^{\parallel},x_0,\delta)$ adopting the relation $\rho_{Si}^{\parallel}=\rho_{Si}^{\perp}$. Since $f(\alpha_{FM}^{\perp},x_0,\delta)/f(\alpha_{FM}^{\parallel},x_0,\delta)>1$, the AMV of Si is always negative, and increases in magnitude as δ grows. The maximal AMV will be:

$$\mathrm{AMV}=1-\frac{\alpha_{FM}^{\parallel}\left(1+w\alpha_{FM}^{\parallel}\right)}{\alpha_{FM}^{\perp}\left(1+w\alpha_{FM}^{\perp}\right)}\exp\left[\left(\alpha_{FM}^{\parallel}-\alpha_{FM}^{\perp}\right)x_0\right] \quad (5)$$

obtained in the limit of $x\to\infty$ and $L\to\infty$. According to Equation 5, there is a relation AMV(Si) > AMV(FM) for sufficiently large x_0, i.e., the non-magnetic Si seems more susceptible than the FM layer to the magnetic field. This inference is consistent with the experiment results in Figure 2e and 2f.

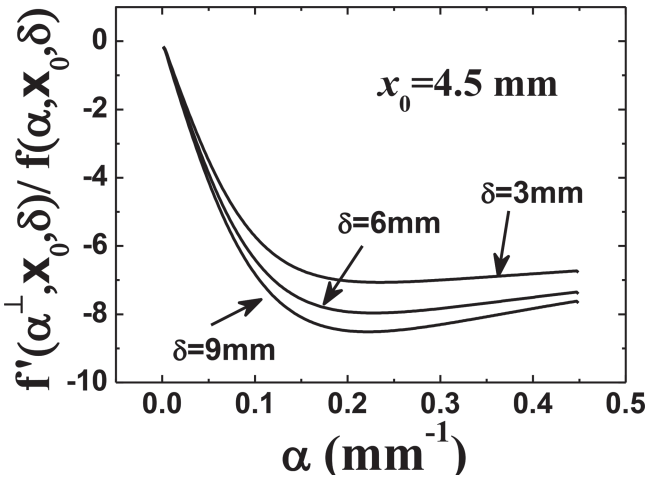

Figure 5. Variation of $f'(\alpha_{FM}^{\perp},x_0,\delta)/f(\alpha_{FM}^{\perp},x_0,\delta)$ with $\alpha^{\perp}$, where x_0 has been set to 4.5 mm and δ to 3, 6 and 9 mm.

It is easy to prove that $\frac{\alpha}{\alpha_{FM}^{\parallel}}=\frac{\alpha_{FM}^{\parallel}-\alpha_{FM}^{\perp}}{\alpha_{FM}^{\parallel}}<\frac{1}{2}\frac{\rho_{FM}^{\parallel}-\rho_{FM}^{\perp}}{\rho_{FM}^{\parallel}}$, i.e., $\alpha^{\parallel}$ and $\alpha^{\perp}$ are very close to each other (the AMR of the FM layer is generally only a few percent). Therefore, for Si, Equation 4 can be further simplified to:

$$\mathrm{AMV}=1-\frac{f(\alpha_{FM}^{\perp},x_0,\delta)}{f(\alpha_{FM}^{\parallel},x_0,\delta)}\approx\frac{f'(\alpha_{FM}^{\perp},x_0,\delta)}{f(\alpha_{FM}^{\perp},x_0,\delta)}\Delta\alpha \quad (6)$$

In **Figure 5**, we present the variation of $f'(\alpha_{FM}^{\perp},x_0,\delta)/f(\alpha_{FM}^{\perp},x_0,\delta)$ with $\alpha_{FM}^{\perp}$ by setting x to 4.5 mm and δ to 9 mm. According to Figure 5, $f'(\alpha_{FM}^{\perp},x_0,\delta)/f(\alpha_{FM}^{\perp},x_0,\delta)$ linearly increases with $\alpha_{FM}^{\perp}$ when $\alpha_{FM}^{\perp}$ < 0.15 and slightly decreases when $\alpha_{FM}^{\perp}$ > 0.2. According to Table 1, $\alpha_{FM}^{\perp}$ is near or above 0.2 for FM/p-Si and well below 0.1 for FM/n-Si(1) (except for Ta/Nc/Ta/n-Si(1)), i.e., the $f'(\alpha_{FM}^{\perp},x_0,\delta)/f(\alpha_{FM}^{\perp},x_0,\delta)$ is larger for FM/p-Si than for FM/n-Si(1). This explains why the AMV of FM/p-Si(1) is generally large. Meanwhile, since Ta has a work function similar to that of n-Si(1), the leakage current of the Ta/NC/Ta/n-Si(1) junction is the highest, i.e., $\alpha^{\perp}$ will be large for this junction. As shown in Figure 2f, we gained a larger AMV by inserting a non-magnetic Ta buffer layer between n-Si(1) and NC. According to Equation 6, not only $\alpha_{FM}^{\perp}$ but also $\Delta\alpha$ will affect the AMV. For the Py/n-Si(2) junction, the AMV is negligibly small since the $\Delta\alpha$ of this junction is 100-fold lower than that of the other junctions. Therefore, to enhance the AMV of Si, the interfacial barrier should be low, which favors a large $\alpha_{FM}^{\perp}$, and the resistivity of the Si substrate should be low, which gives rise to a large $\Delta\alpha$ according to Equation 3.

In summary, the magnetic effect on the photovoltaic effect of the FM/Si junction has been studied (FM = Py, NC, and Ta/NC/Ta). It is found that the lateral photovoltage of either the FM layer or the Si substrate is strongly coupled to the magnetic

alignment of the FM layer, and an anisotropic magnetic photovoltaic effect appears when the magnetic moment reorients in the magnetic field. Moreover, the AMV is much larger for the Si substrate than for the FM layer, and can be modified by very low magnetic fields, on the order of oersteds. The planar Hall effect generated by the photocurrent, a transverse photovoltaic effect, is also observed. This work demonstrates the combined effect of magnetic field and photoexcitation, and may lead to a potential approach for the magnetic tuning of conventional semiconductors.

Experimental Section

Samples were prepared by depositing, via magnetron sputtering in a 0.5 Pa Ar atmosphere, a 20-nm-thick Py film, a 40-nm-thick $Ni_{65}Co_{35}$ film, and a Ta(4nm)/$Ni_{65}Co_{35}$(40nm)/Ta(4nm) (Ta/NC/Ta) trilayer on different (001)-Si substrates (10 mm × 20 mm in size) through a Hall bar-shaped mask. The film thickness was calibrated by low-angle X-ray reflectivity. To define the magnetic easy axis, a magnetic field was applied along the short axis of the film (*y*-axis) during film deposition. Three kinds of Si substrates have been employed, with a hole density of ca. 1×10^{15} cm^{-3} (p-Si), an electron density of ca. 2×10^{14} cm^{-3} (n-Si(1)), and an electron density of 10^{12} cm^{-3} (n-Si(2)). A NanoVoltmeter (Keithley 2182A) was used for the photoelectrical measurements. Silver paint and aluminum ultrasonic bonding were, respectively, used for electric connections of the FM film and the Si substrate. To get an Ohmic Si–Al contact, a voltage pulse of 80 V was applied to break the possible interfacial barrier. A laser beam with a wavelength of 635 nm and a power of 30 mW was used to excite the electron–hole pairs in Si. The entire sample, except for the illuminated region, was covered by an opaque soft mask during the measurements, and all the experiments were conducted under ambient conditions. The finite element analysis technique was used to simulate the spatial distribution of the electric potential in the Si substrate when the above FM layer was illuminated by a laser, based on the charge density determined by the Poisson equation and Equation 2.

Supporting Information

Supporting Information is available from the Wiley Online Library or from the author.

Acknowledgements

This work was supported by the National Basic Research of China, the National Natural Science Foundation of China, the Knowledge Innovation Project of the Chinese Academy of Science, and the Beijing Municipal Nature Science Foundation.

Received: August 24, 2014
Published online: October 27, 2014

[1] a) I. Appelbaum, B. Huang, D. J. Monsma, *Nature* **2007**, *447*, 295; b) M. Xiao, I. Martin, E. Yablonovitch, H. W. Jiang, *Nature* **2004**, *430*, 435; c) R. Fiederling, M. Keim, G. Reuscher, W. Ossau, G. Schmidt, A. Waag, L. W. Molenkamp, *Nature* **1999**, *402*, 787; d) R. Jansen, *Nat. Mater* **2012**, *11*, 400.
[2] G. Lampel, *Phys. Rev. Lett.* **1968**, *20*, 491.
[3] a) S. P. Dash, S. Sharma, R. S. Patel, M. P. de Jong, R. Jansen, *Nature* **2009**, *462*, 491; b) B. T. Jonker, G. Kioseoglou, A. T. Hanbicki, C. H. Li, P. E. Thompson, *Nat. Phys* **2007**, *3*, 542; c) B. C. Min, K. Motohashi, C. Lodder, R. Jansen, *Nat Mater* **2006**, *5*, 817.
[4] K. Ando, E. Saitoh, *Nat. Commun* **2012**, *3*, 629.
[5] J. C. Le Breton, S. Sharma, H. Saito, S. Yuasa, R. Jansen, *Nature* **2011**, *475*, 82.
[6] Y. K. Kato, R. C. Myers, A. C. Gossard, D. D. Awschalom, *Science* **2004**, *306*, 1910.
[7] M. Yamanouchi, D. Chiba, F. Matsukura, H. Ohno, *Nature* **2004**, *428*, 539.
[8] C. Wan, X. Zhang, X. Gao, J. Wang, X. Tan, *Nature* **2011**, *477*, 304.
[9] M. P. Delmo, S. Yamamoto, S. Kasai, T. Ono, K. Kobayashi, *Nature* **2009**, *457*, 1112.
[10] J. J. H. M. Schoonus, F. L. Bloom, W. Wagemans, H. J. M. Swagten, B. Koopmans, *Phys. Rev. Lett.* **2008**, *100*, 127202.
[11] a) D. Yang, F. Wang, Y. Ren, Y. Zuo, Y. Peng, S. Zhou, D. Xue, *Adv. Funct. Mater.* **2013**, *23*, 2918; b) T. Wang, M. Si, D. Yang, Z. Shi, F. Wang, Z. Yang, S. Zhou, D. Xue, *Nanoscale* **2014**, *6*, 3978; c) M. P. Delmo, S. Kasai, K. Kobayashi, T. Ono, *Appl. Phys. Lett.* **2009**, *95*; d) Z. G. Sun, M. Mizuguchi, T. Manago, H. Akinaga, *Appl. Phys. Lett.* **2004**, *85*, 5643.
[12] a) T. R. Mcguire, R. I. Potter, *Ieee. T. Magn* **1975**, *11*, 1018; b) F. J. Himpsel, J. E. Ortega, G. J. Mankey, R. F. Willis, *Adv. Phys* **1998**, *47*, 511.
[13] B. G. Toth, L. Peter, A. Revesz, J. Padar, I. Bakonyi, *Eur. Phys. J. B* **2010**, *75*, 167.
[14] a) K. J. Jin, H. B. Lu, K. Zhao, C. Ge, M. He, G. Z. Yang, *Adv. Mater* **2009**, *21*, 4636; b) W. Schottky, *Phys. Z.* **1930**, *31*, 913; c) J. Henry, J. Livingstone, *Adv. Mater.* **2001**, *13*, 1023; d) J. Henry, J. Livingstone, *J. Phys. D: Appl. Phys.* **2008**, *41*.
[15] H. Niu, T. Matsuda, H. Sadamatsu, M. Takai, *Japan. J. Appl. Phys.* **1976**, *15*, 601.